

Internal Calibration System Using Learning Algorithm With Gradient Descent

Chan-Yong Jung¹, Kyung-Bin Bae, Dong-Chan Kim¹, and Seong-Ook Park¹, *Senior Member, IEEE*

Abstract—We present a novel approach to internal calibration of a radar system. A Ku-band radar system with internal calibration paths is designed. Thermal drift of a system is mainly caused by active components, which are a high-power amplifier (HPA) and a low-noise amplifier (LNA). We aimed to reduce the drift using a learning algorithm with a gradient-descent method. Hardware offset factors and calibration factors are introduced for the process. In the learning algorithm, a penalty term is formed based on the analysis of local minimum points. The result verifies the proposed internal calibration method. Maximum deviations of gain are 0.0477 dB for the HPA and 0.0132 dB for the LNA. In addition, the maximum deviations of phase are 0.2481° for HPA and 0.0722° for LNA, respectively.

Index Terms—Calibration, gradient descent, internal calibration, Ku-band, synthetic aperture radar (SAR).

I. INTRODUCTION

THE synthetic aperture radar (SAR) system obtains image data of the earth's surface using reflected echoes of a signal. During the data acquisition, a systematic error arises because of thermal drift and aging of hardware components. Moreover, in an in-flight environment, the system needs to minimize these errors itself. Therefore, radiometric calibration is essential to ensure high quality of data [1]–[5].

Radiometric calibration can be divided into two categories: internal and external calibration. Internal calibration monitors the instrumental drift within a system using calibration signals that are usually calibration tones or chirp replicas. Comparing the system performance with a reference predefined system, the system deviation is reduced [1].

External calibration reduces the deviation using known ground targets, such as the corner reflector, transponder, and natural terrain [2]. Variations of components that are not included in the internal calibration loop can be removed.

Manuscript received March 22, 2019; revised September 18, 2019; accepted October 26, 2019. Date of publication November 14, 2019; date of current version August 28, 2020. This work was supported by an Institute for Information and Communications Technology Promotion (IITP) grant funded by the Ministry of Science, Information, and Communication Technology (MSIT), South Korea, under Grant 2018-0-01658 and Grant 2018-0-00733, in part by the Key Technologies Development for Next Generation Satellites, and in part by the Development of Testing and Verification Technology for 5G Mobile Communications supporting enhanced mobile broadband (eMBB), ultra reliable/low latency communication (URLLC), and machine-type communications (mMTC). (*Corresponding author: Chan-Yong Jung.*)

The authors are with the Microwave and Antenna Laboratory, School of Electrical Engineering, Korea Advanced Institute of Science and Technology (KAIST), Daejeon 34141, South Korea (e-mail: jcy132@kaist.ac.kr; carrier-bkb@kaist.ac.kr; kdch5204@kaist.ac.kr; soparky@kaist.ac.kr).

Color versions of one or more of the figures in this letter are available online at <http://ieeexplore.ieee.org>.

Digital Object Identifier 10.1109/LGRS.2019.2950671

1545-598X © 2019 IEEE. Personal use is permitted, but republication/redistribution requires IEEE permission. See <https://www.ieee.org/publications/rights/index.html> for more information.

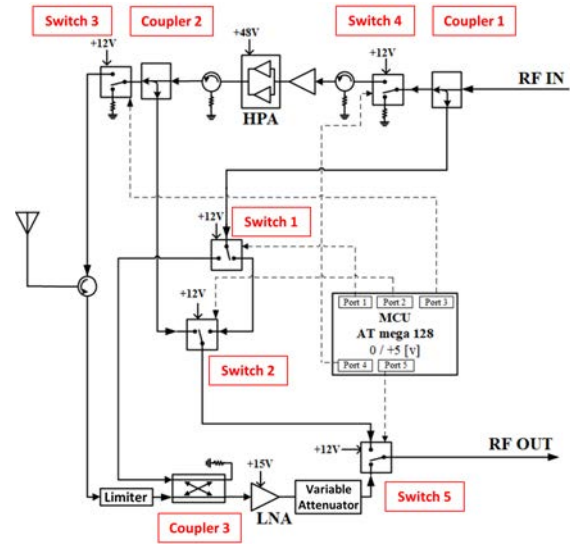


Fig. 1. Internal calibration network.

To achieve a less deviation of a radar system performance, various internal calibration methods were studied [1]–[8]. Del Castillo Mena and Larrañaga Sudepe [2] analyzed a calibration system in the Spanish National Institute of Aerospace Technology (INTA) SAR system with a chirp replica, which recorded 0.7 dB and 5° resolution, and Younis *et al.* [4] implemented a calibration system using an extra calibration tone in multichannel SAR, which recorded phase resolution of less than 1° . Bräutigam *et al.* [8] developed internal calibration for TerraSAR-X using pulse sequences, which recorded 0.16 dB and 2° resolution.

This letter proposes a novel approach to an internal calibration method for a radar system that uses a learning algorithm with a gradient-descent method. A Ku-band system that contains an internal calibration network is implemented to verify the calibration process. Hardware offset factors and calibration factors are newly defined for the process. In the learning algorithm, we set a penalty function based on an analysis of local minima. Our results suggest that the system drift is adjusted with low deviation.

II. INTERNAL CALIBRATION NETWORK

A. Internal Calibration Network

The implemented internal calibration network is shown in Fig. 1. There are three calibration signal paths for three different calibration modes: P1–P3 modes.

TABLE I
THEORETICAL VALUES FOR LEAKAGE ANALYSIS

	P1 Mode	P2 Mode	P3 Mode
P1 Path (dBm)	-31	-205	-149
P2 Path (dBm)	-143	-28	-143
P3 Path (dBm)	-95	-151	-36
TRx Path (dBm)	-99	-102	-158
Measurement (dBm)	-31.26	-32.22	-40.68

In the P1 mode, a calibration signal passes through the high-power amplifier (HPA) and monitors the drift of the HPA. The path follows Coupler1 Switch4 Coupler2, Switch2, and Switch5 as marked in Fig. 1. In the P2 mode, the signal passes the low-noise amplifier (LNA) and monitors the drift of the LNA. The path follows Coupler1, Switch1, Coupler3, and Switch5. In the P3 mode, the signal follows the path that does not include the LNA and HPA. The path follows Coupler1, Switch1, Switch2, and Switch5.

B. Leakage Analysis

In practice, a small portion of a signal can leak out through a disconnected path in the switch. If a leakage signal passes the amplifier, it can distort the main signal. Therefore, it is essential to analyze the leakage signals within the system.

The signal path for each calibration mode can be a leakage signal path. There can also be a leakage signal, which follows Coupler1, Switch4, Coupler2, Switch3, Isolator Coupler3, and Switch5, which will be denoted as p_{TRx} in this letter.

For the analysis, specifications of system elements are denoted by simple symbols. As shown in Fig. 1, five switches are indexed. For the switch with index number n , the insertion loss is set as s_n and the isolation is set as i_n . The isolation of a circulator is marked as i_{cir} . Three couplers are numbered, as shown in Fig. 1. For the coupler with index number n , the insertion loss is set as l_n , and the coupling factor is set as c_n . The insertion loss of the attenuator is marked as L . The gain of HPA and LNA is set as g_H and g_L , respectively.

The leakage analysis for the system in the P1 mode is introduced as an example. Let the calibration signal at each mode be $p1$ – $p3$ with the input signal p .

The main signal can be formulated as

$$p1(t) = p(t) * l_1 * s_4 * g_H * c_2 * s_2 * s_5 \quad (1)$$

and three leakage signals can be formulated as

$$p2_{\text{leak}}(t) = p(t) * c_1 * i_1 * c_3 * g_L * L * i_5 \quad (2)$$

$$p3_{\text{leak}}(t) = p(t) * c_1 * s_1 * i_2 * s_5 \quad (3)$$

$$p_{\text{TRx,leak}}(t) = p(t) * l_1 * s_4 * g_H * l_2 * i_3 * i_{\text{cir}} * l_3 * g_L * i_5. \quad (4)$$

The analysis is also applicable to P2 and P3 modes. The experimental result is shown in Table I. It demonstrates the robustness of the system to leakage signals. Detailed explanation of the experiment is in Section V.

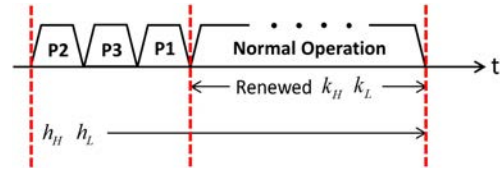


Fig. 2. One cycle of system operation.

III. INTERNAL CALIBRATION

Using the previous analysis, the gain and phase of the HPA and the LNA can be expressed with the calibration signal along with the parameters of the passive components

$$g_H = \frac{p1}{p3} * \frac{c_1 s_1}{l_1 s_4 c_2} \quad g_L = \frac{p2}{p3} * \frac{s_2}{c_3 L} \quad (5)$$

$$\phi_H = \angle p1 - \angle p3 + \theta_H \quad \phi_L = \angle p2 - \angle p3 + \theta_L. \quad (6)$$

In (6), θ_H and θ_L are constant terms related only to phase shifts within passive elements. It is known that the active components mainly cause instrumental drift, rather than the passive components [1], [7]. Therefore, the parameters of passive components can be treated as fixed values. At this point, it is certain that the system drift can be monitored with calibration signals.

Section III-A explains how the proposed internal calibration is designed to reduce system deviation.

A. Proposed Internal Calibration Procedure

The procedure of the proposed internal calibration is divided into four stages. The first stage sets the initial reference state of the system, which refers to the ideal system performance where there is no system drift.

In the second stage, the hardware offset factor is obtained to remove hardware errors that are caused by hardware imperfections, such as nonideal impedance matching and loss in system components. Now, the system is ready to operate.

In the third stage, the system operates as shown in Fig. 2. The system has four operation modes, three calibration modes, and the normal operation mode. The calibration signals are measured periodically in calibration modes to monitor the system drift. In the normal operation, the system works as a radar system.

The last stage is the signal compensation stage. Calibration factors are computed and applied to a signal, which is acquired in normal operation, as shown in Fig. 2. As a result, the signal that is distorted by system drift is compensated for. Note that the calibration factors k_H and k_L are updated in every cycle, while hardware offset factors h_H and h_L are not. The procedure for the signal compensation is introduced in Section IV.

1) *Hardware Offset Factors h_H and h_L* : In practice, there is a gap between (5) and measured data. Therefore, (7) is formulated for experimental purposes. Here, hardware offset factors h_L and h_H are newly defined and applied to the modified equation

$$g_H = \frac{p1_{\text{main}}}{p3_{\text{main}}} * h_H \quad g_L = \frac{p2_{\text{main}}}{p3_{\text{main}}} * h_L. \quad (7)$$

Since the hardware imperfection is not related to the system drift, hardware offset factors remain unchanged in the internal calibration procedure.

2) *Calibration Factors k_H and k_L* : The calibration factor is a value, which has a magnitude as the gain deviation and a phase as the phase deviation caused by the system drift. k_H is the calibration factor for the HPA drift, and k_L is the factor for the LNA drift.

Let the changed gain and phase be $g_{H,d}$ and $g_{L,d}$ and $\phi_{H,d}$ and $\phi_{L,d}$ for the HPA and the LNA, respectively. Also, $g_{H,i}$ and $g_{L,i}$ and $\phi_{H,i}$ and $\phi_{L,i}$ indicate the gain and phase of the HPA and LNA at the predefined initial reference state

$$|k_H| = \frac{g_{H,i}}{g_{H,d}} \quad |k_L| = \frac{g_{L,i}}{g_{L,d}} \quad (8)$$

$$\angle(k_H) = \phi_{H,i} - \phi_{H,d} \quad \angle(k_L) = \phi_{L,i} - \phi_{L,d}. \quad (9)$$

From (6) and (7), calibration factors can be computed using the measured calibration signals. In this process, a learning algorithm is used to estimate the waveform of the measured signals.

B. Learning With Gradient Descent

1) *Loss Function*: Since calibration signals are sinusoidal with a single frequency, they can be formulated as (10). In the equation, n refers to the index of the data sample. Unknown amplitude A , period T , and phase θ of the measured signal are determined by the learning algorithm

$$\hat{y}_n = A \cos\left(\frac{2\pi n}{T} + \theta\right). \quad (10)$$

The loss function is defined as (11). y_i is the measured value and \hat{y}_i is the output of the learning algorithm. Penalty term ϕ is added to make the learning algorithm more stable. A learning rule with a momentum gradient descent is applied [9]

$$E = \frac{1}{2m} \sum_{i=1}^m (y_i - \hat{y}_i)^2 + \mu\phi. \quad (11)$$

2) *Penalty Function*: There are many local minimum points in the loss surface. In both positive and negative A regions, minimum points are periodically located at every 2π interval in the θ dimension. The minimum points are also located in the negative T region symmetrically.

However, for a stable convergence of the algorithm, it is preferable to have only one global minimum point. Therefore, we suggest four constraints to remove redundant points

$$g1 = A_{\text{barrier}} - A < 0 \quad (12)$$

$$g2 = T_{\text{barrier}} - T < 0 \quad (13)$$

$$g3 = -\pi + \theta < 0 \quad (14)$$

$$g4 = -\pi - \theta < 0. \quad (15)$$

With these constraints, the penalty term ϕ is formulated in (16). Then, the algorithm can converge to the global minimum point while satisfying the constraints

$$\phi = (\max[0, g1])^2 + (\max[0, g2])^2 + (\max[0, g3])^2 + (\max[0, g4])^2. \quad (16)$$

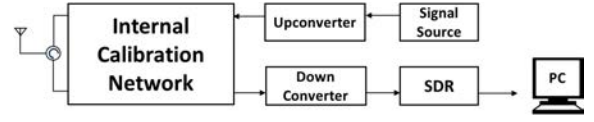


Fig. 3. Overall internal calibration system.

3) Evaluation of the Learning Algorithm:

1) *Error Rate*: A concept that quantifies the reliability of the algorithm is newly defined. In (17), E denotes the loss function and A denotes the amplitude of the main signal. It is able to determine that $\sqrt{2E}$ is the standard deviation of the trained model resulting from the algorithm

$$\text{Error rate} = \frac{\sqrt{2E}}{A}. \quad (17)$$

The error rate measures the ratio of error to the main signal. A small value of the error rate indicates that the trained model well represents the measured data.

2) *Learning Speed Estimation*: The speed of convergence is an indicator of the learning speed. The first learning epoch, when the loss function becomes less than 1% of the initial value, is used to compare the learning speed. A small value indicates that the learning speed is fast.

C. Verification of Proposed Internal Calibration

As mentioned earlier, the system drift is mainly caused by active components, which are the HPA and LNA in the system [7]. Therefore, calibration signals $p1$ and $p2$ can be distorted by the system drift. To verify the calibration method, we compensated $p1$ and $p2$ using computed calibration factors. In (18), $p1_{\text{drift}}$ and $p2_{\text{drift}}$ denote the distorted signals. $p1_{\text{comp}}$ and $p2_{\text{comp}}$ denote the compensated signals

$$p1_{\text{comp}} = p1_{\text{drift}} * k_H \quad p2_{\text{comp}} = p2_{\text{drift}} * k_L. \quad (18)$$

Then, we computed the deviation of the gain and phase of each active component and observed how they change. In (19), g and ϕ are the computed gain and phase. g_{initial} and ϕ_{initial} are the gain and phase of active components within the system in the initial reference state

$$\Delta g = g - g_{\text{initial}} \quad \Delta\phi = \phi - \phi_{\text{initial}}. \quad (19)$$

If the value of each deviation approaches 0, we can conclude that the proposed method is valid. Our result verified the method, showing that the deviations are much reduced.

IV. KU-BAND INTERNAL CALIBRATION SYSTEM

The Ku-band internal calibration system is shown in Fig. 3. The upconverter converts a 140-MHz signal to 14 GHz. The downconverter converts a 14-GHz signal to 140 MHz. Software-defined radio (SDR) converts a 140-MHz signal to 890 kHz and samples the signal. The sampled data are processed in a computer, as shown in Fig. 4.

The calibration signals are measured for the initial reference state of the system. Differences in magnitude and phase between calibration signals are shown in Table II. Then, it is enough to compute the gain and phase for each of the active

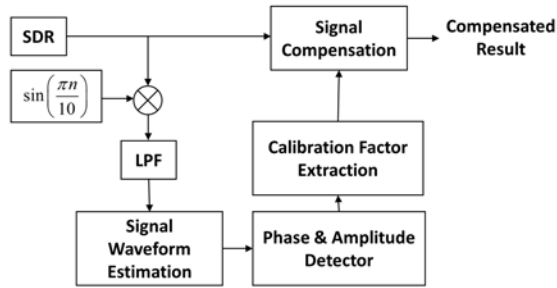


Fig. 4. Diagram of signal processing.

TABLE II
INITIAL REFERENCE STATE OF SYSTEM

	Magnitude Difference	Phase Difference
HPA-Cal	7.09dB	142.473°
LNA-Cal	8.46dB	41.13°

components using (5) and (6). In Table II, HPA-Cal denotes the differences between p_1 and p_3 . LNA-Cal denotes the differences between p_2 and p_3 . In the reference state, the gain of the HPA is 16.48 dB at 37.1 °C, and the gain of the LNA is 48.26 dB at 31.9 °C.

V. RESULTS

A. Hardware Offset

Hardware offset factors are calculated based on Section III. In the theoretical analysis of the system, insertion loss and isolation of switch were set as -1 and -60 dB, respectively. For coupler c_1 shown in Fig. 1, the coupling factor is -10 dB and the insertion loss is 0 dB. The other two couplers have a coupling factor of -20 dB and an insertion loss of 0 dB. For the circulator, the isolation is -20 dB. The loss of the input port cable and output port cable of the measurement equipment is set as -2 and -4 dB, respectively. The power of the input signal is -20 dBm. The measurement results and theoretical values are shown in Table I with a dBm scale.

The offset factors are derived from the results. h_H is 7.06 and h_L is 39.8.

B. Calibration Factor Computation

Calibration factors are computed repeatedly as the temperature changes. In this section, results are shown to explain the procedure for the computation in detail.

The data in this section are acquired with -40 -dBm system input, when the HPA is at 44.9 °C and the LNA is at 45 °C. In the graphs, the blue line represents measured data, and the red dashed line represents the output of the learning algorithm.

For the calculation of k_L , waveforms of p_2 and p_3 signals are estimated using the learning algorithm, as shown in Fig. 5(a) and (b). The error rate for p_2 signal estimation is 3.6458%. For the p_3 signal, the error rate is 1.5115%. k_L is computed from the results: $k_L = 1.0268 \angle -5.0017^\circ$.

The same process is applied to compute k_H . Fig. 6(a) and (b) shows the waveform estimation for the calculation of k_H . The error rate for p_3 signal estimation is 3.4967%. For the

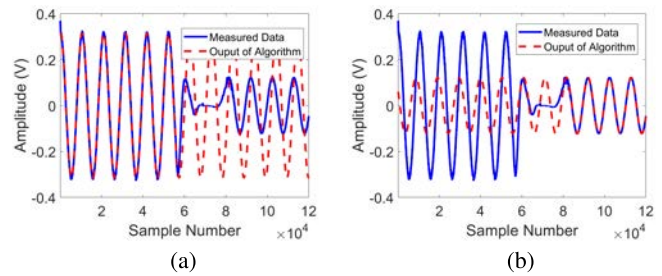
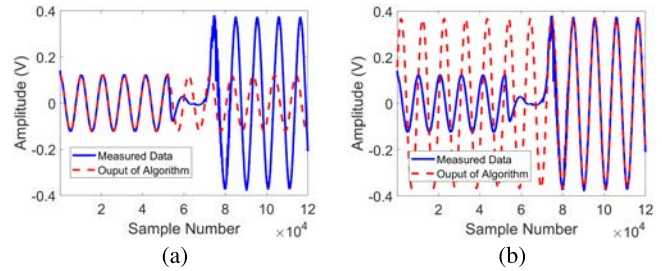
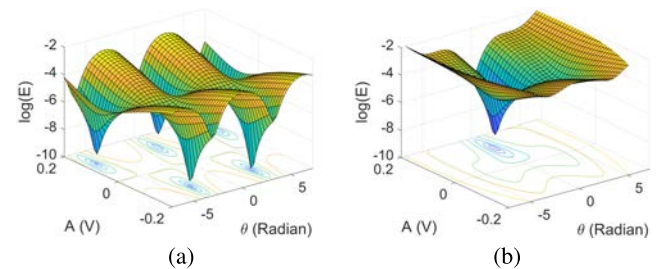
Fig. 5. Learning process for LNA drift monitoring. (a) Learning for p_2 signal. (b) Learning for p_3 signal.Fig. 6. Learning process for HPA drift monitoring. (a) Learning for p_3 signal. (b) Learning for p_1 signal.

Fig. 7. Loss surface of the learning algorithm. (a) Without penalty term. (b) With penalty term.

TABLE III
RESULT OF ALGORITHM

	Without Penalty	With Penalty
Error Rate (%)	3.49267	3.4872
Amplitude (V)	-0.1223	0.1222
Phase (°)	-172.5	7.42
Learning Speed (Epoch)	600	42

p_1 signal, the error rate is 1.45%. The calibration factor for the HPA drift is computed: $k_H = 0.9776 \angle 1.0376^\circ$.

C. Effect of Penalty Term

Two learning algorithms are implemented with the same learning rate, the starting point, and the momentum. One has a penalty term on its loss function, and the other does not. The data are obtained under the conditions of the HPA at 41 °C and the LNA at 34 °C.

The loss surface is visualized in A and θ dimensions with the optimal value of T fixed. As shown in Fig. 7(a), the minimal points are located at the predicted locations.

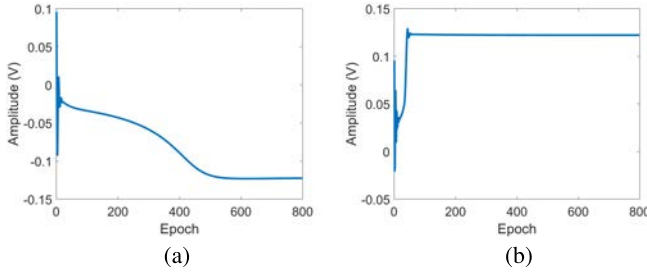


Fig. 8. Learning progress for amplitude estimation. (a) Without penalty term. (b) With penalty term.

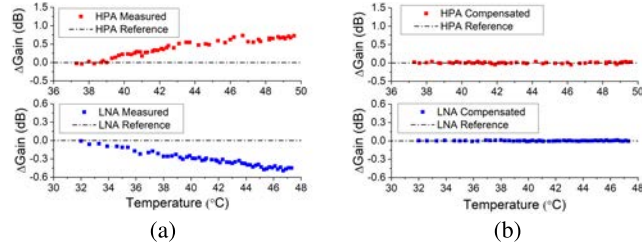


Fig. 9. Gain deviation of the HPA and the LNA. (a) Before compensation. (b) After compensation.

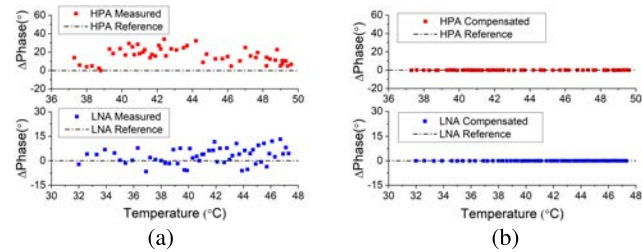


Fig. 10. Phase deviation of the HPA and the LNA. (a) Before compensation. (b) After compensation.

Also, as shown in Fig. 7(b), the redundant minimal points are removed by the penalty function.

Table III and Fig. 8 show the effect of the penalty term. The algorithm that does not have a penalty term converges to the local minimum. In contrast, the algorithm with a penalty term converges to the intended minimum point, while maintaining the same error rate.

It is also remarkable that the penalty term improves the learning speed, removing the influence of local minimum points.

D. Compensation of Signal

This section shows the results of signal compensation. In each figure, the top graph represents the result of the HPA and the bottom graph represents the result of the LNA.

Fig. 9(a) and (b) shows the compensation of gain deviation. After compensation, maximum deviations are 0.0477 dB for the HPA and 0.0132 dB for the LNA.

Fig. 10(a) and (b) shows the compensation of the phase deviation. After compensation, the maximum deviations are 0.2481° for the HPA and 0.0722° for the LNA.

The result suggests that the proposed internal calibration process is valid.

VI. CONCLUSION

We presented a novel approach to internal calibration, which applied learning algorithm with a gradient descent. We newly defined hardware offset factors and calibration factors to reduce the system deviation that is caused by thermal drift. A learning algorithm was employed to compute the calibration factors. Based on our analysis for local minimum points in the loss surface, we suggested a penalty term to improve the algorithm. A Ku-band internal calibration system was designed to verify the proposed method experimentally. The result confirms that the proposed internal calibration method is valid. It is expected that the proposed method can be widely used for a single frequency signal. The development of the method for chirp and frequency modulated continuous wave (FMCW) signals can be considered as a future work.

REFERENCES

- [1] E. Makhoul, A. Broquetas, F. Lopez-Dekker, J. Closa, and P. Saameno, "Evaluation of the internal calibration methodologies for spaceborne synthetic aperture radars with active phased array antennas," *IEEE J. Sel. Topics Appl. Earth Observ. Remote Sens.*, vol. 5, no. 3, pp. 909–918, Jun. 2012.
- [2] J. del Castillo Mena and J. R. L. Sudupe, "Design, performance and calibration review of RBX. INTA new polarimetric SAR system," in *Proc. Eur. Radar Conf.*, Oct. 2013, pp. 235–238.
- [3] Y. Deng, H. Zheng, R. Wang, J. Feng, and Y. Liu, "Internal calibration for stepped-frequency chirp SAR imaging," *IEEE Geosci. Remote Sens. Lett.*, vol. 8, no. 6, pp. 1105–1109, Aug. 2011.
- [4] M. Younis, C. Laux, N. Al-Kahachi, P. Lopez-Dekker, G. Krieger, and A. Moreira, "Calibration of multi-channel spaceborne SAR—Challenges and strategies," in *Proc. 10th Eur. Conf. Synth. Aperture Radar (EUSAR)*, Jun. 2014, pp. 1–4.
- [5] D.-C. Kim, S.-J. Park, T.-W. Kim, L. Minz, and S. Park, "Fully digital beamforming receiver with a real-time calibration for 5G mobile communication," *IEEE Trans. Antennas Propag.*, vol. 67, no. 7, pp. 3809–3819, Jul. 2019.
- [6] W. Yang, C. Xi, G. Jialong, and J. Kai, "Internal and external calibration of POLINSAR," in *Proc. IEEE CIE Int. Conf. Radar*, vol. 1, Oct. 2011, pp. 879–882.
- [7] M. Younis *et al.*, "Investigations on the internal calibration of multi-channel SAR," in *Proc. IEEE Int. Geosci. Remote Sens. Symp. (IGARSS)*, Jul. 2017, pp. 5386–5389.
- [8] B. Bräutigam, M. Schwerdt, M. Bachmann, and M. Stangl, "Individual T/R module characterisation of the TerraSAR-X active phased array antenna by calibration pulse sequences with orthogonal codes," in *Proc. IEEE Int. Geosci. Remote Sens. Symp.*, Jul. 2007, pp. 5202–5205.
- [9] B. Kanigoro and A. G. Salman, "Recurrent gradient descent adaptive learning rate and momentum neural network for rainfall forecasting," in *Proc. Int. Seminar Appl. Technol. Inf. Commun. (ISemantic)*, Aug. 2016, pp. 23–26.
- [10] S. O. Haykin, *Neural Networks and Learning Machines*, 3rd ed. Upper Saddle River, NJ, USA: Pearson, 2009.
- [11] E. K. P. Chong and S. H. Zak, *An Introduction to Optimization* (Wiley Series in Discrete Mathematics and Optimization). Hoboken, NJ, USA: Wiley, 2013. [Online]. Available: <https://books.google.co.kr/books?id=iD5s0iKXHP8C>
- [12] A. M. B. Martinez, L. O. Sanchez, and A. P. Rios, "RBX (Band X SAR): Analysis and calibration of Tx/Rx modules," in *Proc. Eur. Radar Conf. (EuRAD)*, Sep./Oct. 2009, pp. 605–608.
- [13] M. Schwerdt, D. Hounam, and M. Stangl, "Calibration concept for the TerraSAR-X instrument," in *Proc. IEEE Int. Geosci. Remote Sens. Symp. (IGARSS)*, vol. 7, Jul. 2003, pp. 4509–4511.
- [14] M. Schwerdt *et al.*, "Independent system calibration of Sentinel-1B," *Remote Sens.*, vol. 9, no. 6, p. 511, Jun. 2017.